
Proceedings Paper:
Ball, E.A. orcid.org/0000-0002-6283-5949 (2018) Portable and low cost channel sounding platform for VHF / UHF IoT propagation research. In: Loughborough Antennas & Propagation Conference (LAPC 2017). The 13th Loughborough Antennas and Propagation Conference, 13-14 Sep 2017, Loughborough, UK. IET . ISBN 978-1-78561-699-0

https://doi.org/10.1049/cp.2017.0226

Portable and Low Cost Channel Sounding Platform for VHF / UHF IoT Propagation Research

E. A. Ball

Dept. Of Electronic and Electrical Engineering, The University of Sheffield, Sheffield,United Kingdom,
e.a.ball@sheffield.ac.uk

Keywords: Channel Sounding, RTL-SDR, Raspberry Pi, VHF, UHF.

Abstract

This paper presents work into realising a cost-effective and portable platform to support Internet of Things (IoT) propagation research at VHF and UHF. The sounding receiver uses a low cost RTL-SDR, Raspberry Pi and touchscreen. The platform runs dedicated channel sounding DSP algorithms written in Python. The resulting platform is a portable and convenient propagation measurement tool, covering 27MHz to 1.7GHz. Initial results from a city measurement campaign at 71MHz and 869.525MHz are presented, showing channel response and interference.

1 Introduction

The Internet of Things (IoT) is now a hot topic in communications research, with a multiplicity of commercial long range proprietary systems being brought to market. Additionally, there are now emerging standards-based systems being developed (notably including the recently ratified NB-IoT and also 802.11ah "HaLow"). Although these various systems are already jockeying for future dominance, there is still much research potential in very low power and low cost IoT long range systems, powered by coin cells (e.g. CR2032) and supporting high-reliability use-cases, with multi-year life expectancy. Such devices could serve in connecting future city infrastructure or ubiquitous social care and healthcare systems.
In the UK, Ofcom has recently promoted the use of VHF spectrum at 55-68MHz / 70.5-71.5MHz / 80.0-81.5MHz for application to IoT [1]. This is in addition to the already popular EU Short Range Devices spectrum (863MHz-870MHz), where many commercial EU IoT radio systems operate.
To facilitate the research for novel future IoT radio systems, which may incorporate multiple RF bands and aspects of configurable modulation and cognitive radio, requires a fundamental understanding of the real-world propagation environment, noise floors and spectrum occupancy.
To support our activities in IoT radio transceiver research, a portable, low cost, frequency-agile channel sounding platform has been created. This allows near-real-time inspection of the channel response in operational environments, such as urban canyons or remote rural locations. The system is built using an RTL-SDR and Raspberry Pi 3B (R-Pi) with touchscreen- all powered by a USB battery power pack.
Use-cases for many long range IoT systems are unlikely to require multi-MHz RF bandwidths, hence the RTL-SDR's maximum RF BW of 2MHz is acceptable for this platform.

2 VHF / UHF Propagation and IoT Use-Cases

The motivation for the creation of the channel sounder platform is to understand the propagation environment in urban and suburban settings, considering multiple RF bands. This will facilitate proposal of novel, high-reliability IoT radio systems of the future. There has been much research into propagation at VHF and UHF bands over the years, for both commercial and military uses (e.g. [2,3]), recently including short range applications [4].
RMS delay spreads in the VHF and UHF bands have been observed to be typically in ranges of 100ns to 2µs at distances of up to 2km in various urban settings [5,6,7] though occasionally reaching 5µs when indoor-outdoor transitions are included [8]. VHF delay spreads in mountainous regions have been seen to reach 8µs[6] to 30µs [9].
In general radio communications, an RMS delay spread of significantly less than the symbol duration does not require equalisation. This is highly advantageous in minimising complexity in an IoT radio. Given that reported RMS delay spreads are typically 2µs or less implies a 20µs symbol duration (or longer) would be advantageous for IoT systems.
However, it is important to characterise various channel propagation scenarios in urban and suburban environments, representing target use-cases, to properly understand the delay spread and channel conditions that may be experienced. Our use-cases of interest are associated with discreet, body-worn, IoT radios. These devices may be used for medical data telemetry, tracking mobile Alzheimer patients or as emergency alarm & fall-detection alert systems. A common feature in health and social care use-cases is the need for the channel response to be evaluated whilst devices are worn and in various positions (standing/sitting/laying on ground).

3 Channel Sounder Hardware

The channel sounding system consists of an RF vector signal generator (operated at a fixed location) and a portable Channel Sounding Receiver (CSR) incorporating a display. An Agilent E4437B signal generator is used as the TX signal source, with arbitrary waveform files created to suit the channel sounding receiver. The hardware used to make the CSR consists of:-

- Raspberry Pi 3B (£34)

- Raspberry Pi 7” touchscreen & case (£76) or 3.5” touchscreen & case (£21)
- NooElec RTL-SDR with 0.5ppm TCXO (£21)
- 5.4Ahr portable USB battery pack (£15)

The overall cost for the portable system (3.5” touchscreen variant) is circa £90, making it extremely cost-effective for both teaching and research in VHF and UHF propagation. The E4437B is a cost-effective RF bench-top 4GHz signal generator, though a suitable bespoke sounding transmitter could be made. The two figures below show the two versions of the Channel Sounding Receiver in operation.

Figure 3.1: RTL-SDR & 7” Touchscreen CSR.

Figure 3.2: RTL-SDR & 3.5” Touchscreen CSR.

In both the above figures the RTL-SDR is the small black oblong device connected via a USB extension lead to the R-Pi and the blue box is the battery pack. The RG316 RF cable is connecting the RTL-SDR to a trial antenna. The use of a USB extension lead allows the RTL-SDR and its associated antenna to be placed as needed, as well as separating it from sources of RF noise in the R-Pi. Ferrite clamps on the cables (not shown) were also found to be essential; further reducing noise from the R-Pi that otherwise desensitises the RTL-SDR.

4 Channel Sounding Algorithm

A BPSK modulated PRBS M-sequence is used to illuminate the channel. The sequence is created in Matlab and an IQ file loaded into the ESG4437B RF signal generator. The CSR runs bespoke DSP code written in Python (initially developed in Matlab). The algorithms are described below.

4.1 PRBS M-Sequence Selection

It is beneficial to keep the CSR Python algorithm complexity low, to support initial development in Matlab as well as future student involvement. A key desire is to avoid the need for any frequency acquisition or code acquisition stages in the CSR. Since the PRBS code is known, no code acquisition is needed. Frequency acquisition can be avoided by recognising that as long as the phase rotation of the RX IQ data (due to frequency errors) is less than 180 degrees over one complete PRBS frame BPSK signals can be demodulated. The relationship between maximum PRBS frame length and overall frequency error (composite of RX and TX) is shown in Equation (1).

$$\pi = \omega_e T_f \qquad (1)$$

In Equation (1), T_f is the duration (seconds) of a single PRBS frame and ω_e is the overall frequency error (rad/s). In the complete system, the worst-case frequency error is 0.5ppm from the RTL-SDR and 1ppm from the ESG4437, leading to a maximum tolerable IF error of 1.5kHz for a 1GHz carrier.
The maximum reliable IQ sampling rate of the RTL-SDR is 2MHz, implying an RF BW of 2MHz could be captured in direct conversion. To obtain maximum possible resolution of propagation reflections, a BPSK bit-rate of 1Mb/s was chosen, thus filling the 2MHz IF BW to the first sinc nulls.
A PRBS-9 M-sequence (511 bits) was chosen, clocked at 1Mb/s, which according to Equation (1) would tolerate IF frequency errors up to 978Hz. Rather than GPS-lock the ESG4437, a small offset correction was implemented to its carrier frequency to ensure that the overall error at the CSR was below 978Hz. Since the ESG4437 internal reference is very stable after warming up, this initial correction approach has proven acceptable for the duration of all measurement campaigns so far. The use of a 511 bit M-sequence leads to a processing gain of 27dB.

4.1 Correlation Technique in Channel Sounding Receiver

Rather than performing the RX sampled signal correlation in the time domain, it is common and more computationally efficient to perform the correlation in the frequency domain [10,11,12], then returning the result to the time domain. The well-known Fast Fourier Transform circular convolution (matched filter) approach employed in the CSR is described in Equation (2).

$$C = IFFT[H(f)^* G(f)] \qquad (2)$$

In Equation (2), *H(f)* and *G(f)* are the Fourier transforms of time series *h(n)* and *g(n)* respectively and * denotes complex conjugation. *C* is the resulting cross-correlation array of the time series, resulting from the Inverse Fast Fourier Transform (IFFT) operation.

Python code controls both the operation of the RTL-SDR and implements the subsequent signal processing algorithms, allowing near-real-time visualisation of the propagation channel delay spread and frequency response.
Data from the RTL-SDR (set to its maximum IF gain of 49dB) holding 32 captured PRBS frames are first stored to file and then processed in Python, leading to graphs of channel impulse and frequency response.
The algorithm employed within the CSR is based on a simplified version of those used in [10,11,12]. In the following descriptions, variables holding arrays of samples are italicised and in ***bold***. Assume there are *N* complex samples per received PRBS frame (length 511, oversampled by factor 2, i.e. *N* = 1022). To facilitate robust detection of at least one strong correlation peak, regardless of time offset, in the captured RX data, the RX data is partitioned into segments of length 2N: ***rx_sequence_2N****[1..2N]*. The overall captured RX data file is then processed in 16 such segments, each of length *2N* samples, using the following pseudo-algorithm (simplified for clarity):

1. Since an FFT input must be periodic in time and the RX data is processed in lengths of 2N, the TX correlation sequence of length N (for matched filtering) must be extended with zeros to length 2N: ***tx_sequence*** = *concatenate* ***[PRBS****, zeros(N)]*
2. The FFT of the time domain TX sequence is then computed: ***T*** = *FFT(****tx_sequence****)*
3. Select segment *K* in turn (0..15) of length *2N* samples from the captured RX data ***rx_data***: ***rx_sequence_2N*** = ***rx_data****[K2N : (K+1)2N-1]*
4. The FFT of *K*th the time domain RX segment is computed: ***R*** = *FFT(****rx_sequence_2N****)*
5. Obtain the conjugate of the frequency domain representation of received data: ***Rconj*** = *conjugate(****R****)*
6. Compute the delay profile for segment *K* by element-wise multiplying ***Rconj*** & ***T*** and taking inverse FFT: ***time_response*** = *IFFT(****Rconj****.****T****)*
7. Compute delay profile magnitude of segment *K*: ***time_response_mag*** = *abs(****time_response****)*

The element-wise time domain samples in ***time_response_mag*** are then summed across each of the *K* frames of data and the composite array plotted: corresponding to the composite impulse response of the channel at that measurement location. (Note that the individual magnitudes of responses are used for combination, since the impulses have a phase rotation due to IF errors, which tends to otherwise reduce the combined SNR.)
FFTs of each of the 16 ***time_response*** arrays contain the frequency domain response of the channel (bins 1..*N* for positive spectrum above carrier and bins *N*+1..*2N* for negative spectrum below carrier). The magnitude of the 16 responses can then be summed to produce a composite frequency response for the measurement location.
It is beneficial to equalise the frequency response produced to remove the BPSK frequency shaping otherwise imposed on the resulting spectrum. In practice, it was found that nonlinearity from the RTL-SDR required the equalisation to be adjustable and based on input signal level. The BPSK frequency domain response, for use in equalisation, at FFT bin *x* out of *N* is given by Equation (3).

$$\boldsymbol{BPSK\_response}[x] = \left|sinc\left(\frac{x}{N}\right)\right|^{n} \qquad (3)$$

From lab characterisation of the RTL-SDR, exponent *n* is selected based on the magnitude of the maximum time domain correlation peak, *Cp,* using Equation (4).

$$n = 0.25\ln(Cp) - 0.1 \quad (if\ Cp<4500) \qquad (4a)$$

$$n = 0.09\ln(Cp) + 1.18 \quad (if\ Cp>4500) \qquad (4b)$$

Cp can also be used to directly represent the RX RF power, with appropriate calibration offset applied.

5 Early Stage Trials and Results

Simulated channel data was used to first test the system. Figure 5.1 shows the extracted impulse response and Figure 5.2 the frequency response of a simulated channel with a primary signal at 100µs offset (for convenience) and reflections with path deltas of 51µs (-5dB) and 102µs (-10dB).

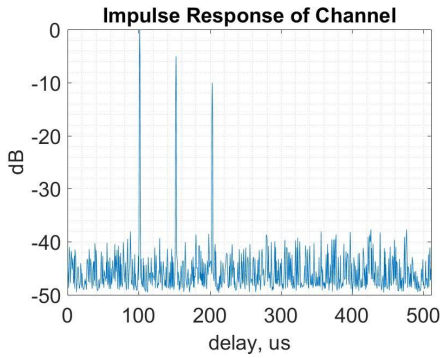

Figure 5.1: Channel impulse response due to 2 simulated reflections at 51µs intervals from a 100µs primary signal.

A reflection with 51µs delay should present itself as spectral peaks and nulls with period 19.6kHz, which is indeed seen in the CSR's spectrum plot in Figure 5.2.

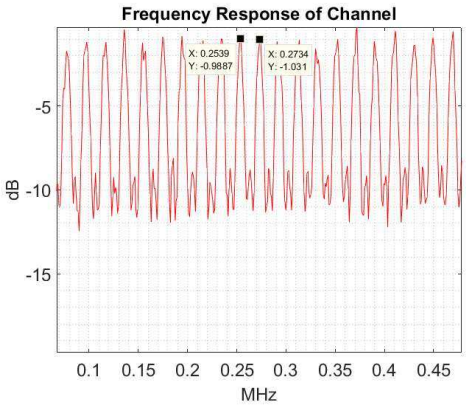

Figure 5.2: Channel frequency response due to 2 simulated reflections at 51µs intervals from a 100µs primary signal.

The measured sensitivity of the CSR is -125dBm at 71MHz and -130dBm at 869.525MHz, for a 10dB correlation peak to noise ratio.
Initial field trials of the CSR in Sheffield city centre have produced interesting results; select examples of which are

reported below. (Note that in all the following time domain plots, the absolute time delay of the primary correlation peak is random, due to random initial M-sequence alignments.) Figures 5.3 and 5.4 show the channel impulse and frequency response, respectively, for in-building measurements at 71MHz (location 3) with the CSR circa 30m from the TX source. The extracted path loss is 100dB.

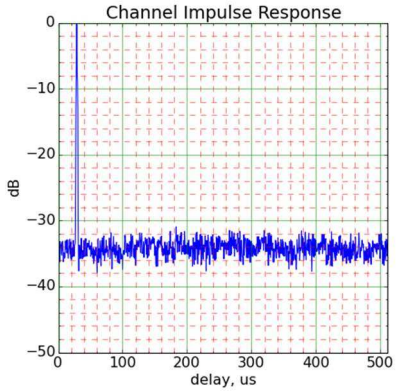

Figure 5.3: 71MHz Channel impulse response (loc'n 3).

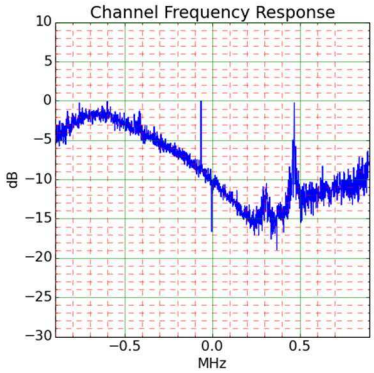

Figure 5.4: 71MHz Channel frequency response (loc'n 3).

Figures 5.5 and 5.6 show channel delay and frequency response, respectively, for measurements at 71MHz at a non-line-of-sight street location (location 8) circa 220m from the indoor sounder TX. The extracted path loss is 120dB. Note the in-band interference on the extracted channel frequency response.

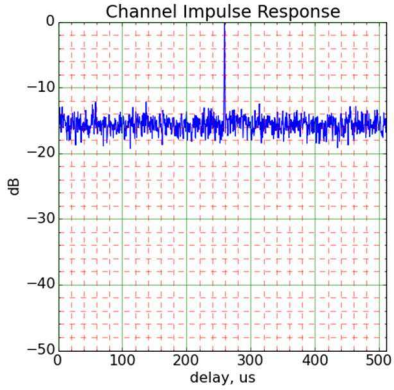

Figure 5.5: (loc'n 8) 71MHz Channel impulse response.

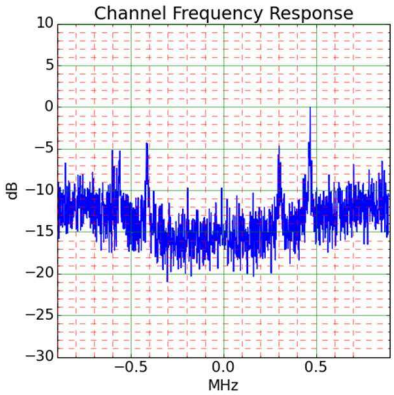

Figure 5.6: 71MHz Channel frequency response (loc'n 8) also showing unknown interference.

Figures 5.7 and 5.8 show the channel delay profile and frequency response, respectively, for in-building measurements at 869.525MHz with the CSR at location 3. The extracted path loss is 89dB.

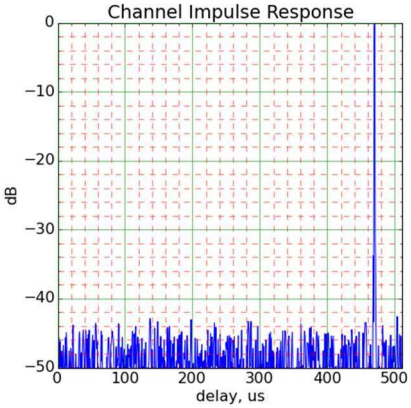

Figure 5.7: 869MHz Channel impulse response (loc'n 3).

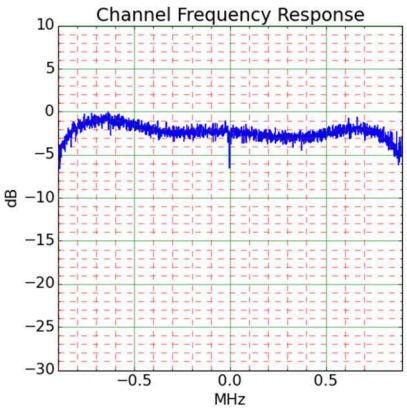

Figure 5.8: 869MHz Channel frequency response (loc'n3).

Figures 5.9 and 5.10 show channel delay and frequency response, respectively, for CSR measurements at 869.525MHz at street location 8 (220m from the indoor TX). The extracted path loss is 127dB.

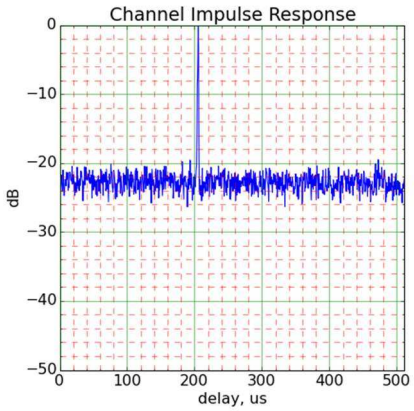

Figure 5.9: 869MHz Channel impulse response (loc'n 8).

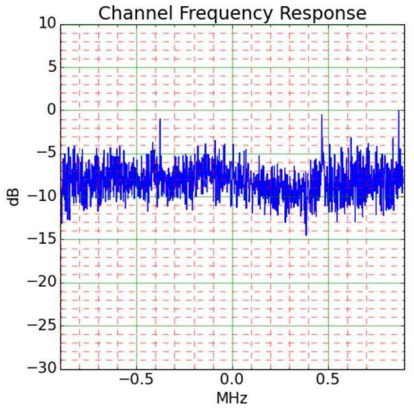

Figure 5.10: 869MHz Channel frequency response (loc'n 8).

Although the delay spreads in the above examples are very low (due to short test site distances), useful and interesting channel frequency responses are still seen.

There were many locations with notable interference present (seen on channel frequency response). During a subsequent investigation, the presence of sources of RF interference at the various test locations was confirmed; with observed RX powers up to -100dBm at 869.5MHz and -80dBm at 71MHz (measured in 10kHz bandwidths).

6 Conclusion and Future Work

This paper shows IoT propagation research (and teaching) can be performed for modest cost. CSR system control is via touchscreen; allowing rapid viewing of channel data in the field and providing insight into the propagation environment and its interaction with any test antennas.

Early testing has shown significant background broadband noise around the 71MHz and 869.525MHz bands (suspected due to various domestic and commercial switched-mode PSUs, PC equipment and LTE band 20 signals). Such RF noise (though real) degrades the sounder's link budget and pollutes the spectral plots. One solution is to increase the processing gain by use of longer M-sequences, though with attendant requirements for more precise oscillators. The bench signal generator limits the portability and cost-effectiveness of the system, hence a bespoke transmitter is now being developed.

The R-Pi platform has proved its suitability for non-real time DSP work. Our next CSR will use a R-Pi controlling a Red Pitaya FPGA board (sampling at 125MHz in I&Q) coupled to a new bespoke RF front-end. This will enable valuable, wider bandwidth, portable propagation measurements to be cost-effectively made for any bands of interest, including future 5G.

References

[1] Ofcom, "VHF radio spectrum for the Internet of Things (Statement)," (2016).

[2] K. Allsebrook and J. D. Parsons, "Mobile Radio Propagation in British Cities at Frequencies in the VHF and UHF Bands," *IEEE Trans. on Vehicular Technologies,* vol. 26, pp. 313-323, (1977).

[3] P. J. Vigneron and J. A. Pugh, "Propagation Models for Mobile Terrestrial VHF Communications," in *MILCOM Conference*, pp. 1-7, (2008).

[4] F. T. Dagefu, G. Verma, C. R. Rao, P. L. Yu, B. M. Sadler, and K. Sarabandi, "Measurement and Characterization of the Short-Range Low-VHF Channel," in *WCNC Conference*, New Orleans, USA, pp. 177-182, (2015).

[5] J. A. Pugh, R. J. C. Bultitude, and P. J. Vigneron, "Mobile Propagation Measurements with Low Antennas For Segmented Wideband Communications at VHF," in *12th ANTEM Conference*, Canada, pp. 1-4, (2006).

[6] J. Fischer, M. Grossmann, W. Felber, M. Landmann, and A. Heuberger, "A Novel Delay Spread Distribution Model for VHF and UHF Mobile-to-Mobile Channels," in *7th EuCAP Conference*, Sweden, pp. 469-472, (2013).

[7] J. A. Pugh, R. J. C. Bultitude, and P. J. Vigneron, "Propagation Measurements and Modelling for Multiband Communications on Tactical VHF Channels," in *MILCOM Conference*, USA, (2007).

[8] M. Karam, W. Turney, K. Baum, P. Sartori, L. Malek, and I. Ould-Dellahy, "Outdoor-Indoor Propagation Measurements and Link Performance in the VHF/UHF Bands," *68th VTC Conference*, Canada, pp.1-5, (2008).

[9] H. Safer, G. Berger, and F. Seifert, "Wideband Propagation Measurements of the VHF-Mobile Radio Channel in Different Areas of Austria," in *5th International Symposium on Spread Spectrum Techniques and Applications*, South Africa, pp. 502-506, (1998).

[10] P. C. Fannin, A. Molina, S. S. Swords, and P. J. Cullen, "Digital Signal Processing Techniques Applied to Mobile Radio Channel Sounding," *IEE Proceedings F - Radar and Signal Processing,* vol. 138, pp. 502-508, (1991).

[11] S. A. Charles, E. A. Ball, T. H. Whittaker, and J. K. Pollard, "Channel Sounder for 5.5GHz Wireless Channels," *IEE Proceedings in Communications,* vol. 150, pp. 253-258, (2003).

[12] M. MacCurdy, R. Gabrielson, E. Spaulding, A. Purgue, K. Cortopassi, and F. K., "Automatic Animal Tracking Using Matched Filters and Time Difference of Arrival," *Journal of Communications,* vol. 4, pp. 487-495, (2009).